# Thermosensitive Nucleosome Editing Reveals the Role of DNA Sequence in Targeted Histone Variant Deposition

**Lu Sun**[1,3], **Leonidas Pierrakeas**[1,3], **Tailai Li**[1], **Ed Luk**[1,2,4,*]

[1]Department of Biochemistry and Cell Biology, Stony Brook University, Stony Brook, NY 11794, USA

[2]Renaissance School of Medicine, Stony Brook University, Stony Brook, NY 11794, USA

[3]These authors contributed equally

[4]Lead Contact

## SUMMARY

In preparation for transcription, the chromatin remodeler SWR installs homotypic ZZ nucleosomes at promoters by replacing the two nucleosomal H2A with H2A.Z in a stepwise manner. Nucleosome-free regions (NFRs) help recruit SWR to promoters; this is thought to position SWR asymmetrically on one side of the +1 nucleosome. How SWR accesses the opposite side of +1 to generate a ZZ nucleosome remains unclear. Using biochemical assays that monitor the sub-nucleosomal position of nascent H2A.Z, we find that NFR-recruited SWR switches sides to insert H2A.Z into asymmetrically positioned nucleosomes; however, at decreasing temperatures, H2A.Z insertion becomes progressively biased for one side. We find that a 16-bp element containing G/C runs (>3 consecutive G or C nucleotides) is sufficient to promote H2A.Z insertion. Because H2A.Z-rich +1 nucleosomes in yeast have more G/C runs, we propose that nucleosome editing is a thermosensitive process that can be hard coded by the genome.

## In Brief

The SWR remodeler edits promoter-proximal +1 nucleosomes by sequentially replacing the two copies of histone H2A with H2A.Z. Sun et al. show that temperature and DNA sequence strongly influence on which side of the nucleosome SWR inserts H2A.Z first, thereby affecting the remodeling outcome.

## Graphical Abstract

## INTRODUCTION

Regulation of DNA accessibility in chromatin is a fundamental mechanism of transcriptional control in eukaryotes and probably in archaea (Kornberg and Lorch, 1999; Mattiroli et al., 2017). The majority of nucleosomes have a histone core comprising 2 H2A-H2B dimers and 1 H3-H4 tetramer with ~150 bp of DNA wrapped around this core and linker DNA protruding on both sides (Luger et al., 1997). In the nucleosome immediately downstream of most promoters, called +1, the variant histone H2A.Z is frequently found in place of H2A (Albert et al., 2007). These H2A.Z-containing nucleosomes are poised for transcription-dependent disassembly and their presence is required for distinct transcriptional responses (Cortijo et al., 2017; Dhillon et al., 2006; Tramantano et al., 2016; Zhang et al., 2005). H2A.Z is inserted into nucleosomes by the SWR complex, which is an ATP-dependent chromatin remodeler made up of 14 different proteins (Kobor et al., 2004; Krogan et al., 2003; Mizuguchi et al., 2004). How SWR unravels the nucleosomal DNA to replace each nucleosomal H2A-H2B (A-B) dimer with an H2A.Z-H2B (Z-B) dimer is a central question of the present study.

Like other members of the super family (SF) 2-class chromatin remodelers, SWR has an ATPase motor that is homologous to translocases known for catalyzing movement along double-stranded DNA (Flaus et al., 2006). Many SF2-class remodelers catalyze nucleosome sliding *in vitro*, an activity defined by repositioning a histone octamer along DNA (Bartholomew, 2014). While remodelers, such as SWI/SNF and RSC, are able to disassemble nucleosomes, SWR does not slide or disassemble nucleosomes (Dechassa et al., 2010; Lorch et al., 2006; Ranjan et al., 2015). Instead, SWR catalyzes a histone exchange reaction that involves the coupled removal of one nucleosomal A-B dimer with the insertion of a Z-B dimer (Luk et al., 2010; Mizuguchi et al., 2004). Canonical AA nucleosomes have two A-B dimers on opposite faces. SWR replaces the A-B dimers with Z-B dimers in a stepwise manner, thereby generating heterotypic AZ nucleosomes as an intermediate and

homotypic ZZ nucleosomes as the final product (Luk et al., 2010). The directionality of an H2A-to-H2A.Z exchange is driven by both the histone-binding modules of SWR that discriminate between H2A and H2A.Z (Hong et al., 2014; Liang et al., 2016; Sun and Luk, 2017) and the regulation of the remodeling ATPase, which is optimally stimulated when SWR binds simultaneously to an H2A-containing nucleosome and a Z-B dimer (Luk et al., 2010).

Although histone exchange and nucleosome sliding are different remodeling outcomes, the ATPase motor of SWR and those of sliding remodelers such as SWI/SNF, RSC, ISWI, and Chd1, engage the nucleosome at a similar site called superhelical location (SHL) 2 (defined as the location 2 helical turns from the nucleosomal dyad) (Dechassa et al., 2008; Nodelman et al., 2017; Ranjan et al., 2015; Saha et al., 2005; Schwanbeck et al., 2004; Zofall et al., 2006) (Figure S1A). One hypothesis is that SWR uses a similar strategy as sliding remodelers to destabilize nucleosomes before a SWR-specific mechanism kicks in to orchestrate histone dimer exchange (Zhou et al., 2016). In nucleosome sliding, the ATPase motor translocates along the "tracking" strand at SHL2 (Figure S1A, cyan), leading to unwinding/overstretching of a DNA segment toward the proximal DNA entry site (Figure S1A, orange arrow) and overwinding toward the dyad (Figure S1A). The histone core conformation deforms to accommodate the DNA distortion (Sinha et al., 2017). The overwound DNA then propagates across the dyad toward the second gyre, presumably as a bulge, which then exits the nucleosome before the linker DNA on the entry site is drawn in to relieve the overstretched region (Deindl et al., 2013). Moreover, recent studies have shown that the sequence of the nucleosomal DNA can modulate remodeler activity, suggesting that remodeling outcomes such as nucleosome sliding and histone eviction along the genome are context dependent (Lorch et al., 2014; Winger and Bowman, 2017).

The targeted deposition of H2A.Z at +1 nucleosomes *in vivo* is mediated in part by the affinity of SWR for nucleosomes with longer DNA linkers, which are provided by the promoter-specific nucleosome-free region (NFR) upstream (in relation to transcription) of +1 nucleosomes (Ranjan et al., 2013; Yuan et al., 2005). Downstream is the +2 nucleosome, which is pushed up against +1 by chromatin remodelers (Krietenstein et al., 2016). Thus, a typical +1 nucleosome is flanked by a longer stretch of free DNA (~80–200 bp) on one side compared to the other side (~20 bp) (Yen et al., 2013). Structural and biochemical studies showed that when SWR preferentially binds to the long linker/NFR of an asymmetrically positioned nucleosome, its ATPase motor simultaneously engages the NFR-distal tracking strand at SHL+2 (where the + sign denotes that this site is further away from the NFR in linear distance than the SHL2 site on the opposite face of the nucleosome) (Figure S1B) (Ranjan et al., 2015; Willhoft et al., 2018). The implication is that the engagement of the ATPase with the NFR-distal site will bias the exchange of one of the two A-B dimers. The asymmetric binding of SWR to the +1 nucleosome therefore raises the question of why there is a substantial amount of ZZ nucleosomes present at the +1 position of most promoters (Luk et al., 2010; Mohan et al., 2018).

In this study, a site-specific chemical cleavage strategy was developed to track the sub-nucleosomal location of nascent H2A.Z inserted by SWR. In combination with a gel mobility assay that reports the copy number of H2A.Z per nucleosome, we confirmed that

SWR deposits H2A.Z onto the same face of the nucleosome engaged by the ATPase motor, ruling out the bulge propagation mechanism used by remodeling sliders. We found that when SWR is recruited asymmetrically to nucleosomal substrates with an NFR on one side, its remodeling ATPase can freely access the tracking strands on both faces of the nucleosome to effect H2A.Z insertion; but at suboptimal reaction temperatures, one face becomes biased. We trace the determinant for the thermosensitive H2A.Z insertion to a 16-bp element within the nucleosomal DNA. Our work reveals that DNA sequence plays a more important role than previously thought in determining the site of H2A.Z insertion.

## RESULTS

### An Improved Strategy to Track Nascent H2A.Z in Nucleosomes Inserted by SWR

To recapitulate H2A.Z insertion *in vitro*, native SWR complex was purified from yeast using an improved methodology called another sequential affinity purification (ASAP). ASAP differs from traditional tandem affinity purification (TAP) in that it uses affinity tags on two different subunits to enrich for intact complexes (Rigaut et al., 1999). Amylose affinity chromatography was used in the first step as the maltodextrin-binding protein (MBP) has fast binding and eluting characteristics, minimizing the exposure time of the immobilized complex to whole-cell extracts (Telmer and Shilton, 2003) (Figure 1A). The MBP tag was fused to the C terminus of the Rvb1 subunit (Rvb1$^{MBP}$), one of the two components of the heterohexameric platform for subunit organization in SWR (Nguyen et al., 2013). Binding of Rvb1$^{MBP}$ to an amylose column pulled down not only SWR but also two other complexes, INO80 and R2TP, as all three complexes share Rvb1 (Figures 1A and 1B, lane 1) (Mizuguchi et al., 2004; Rivera-Calzada et al., 2017; Shen et al., 2003). A 3xFLAG-tagged Swr1 (Swr1$^{FL}$), which is the unique ATPase core subunit of SWR, was targeted for FLAG immunoprecipitation (IP), separating SWR from INO80 and R2TP (Figure 1B). ASAP-purified SWR contained all 14 subunits at the expected stoichiometry (Figure 1B, lane 3) (Luk et al., 2010).

SWR activity was evaluated by an *in vitro* assay that monitors the levels of AA, AZ, and ZZ nucleosomes on the basis of their differential mobilities in native PAGE (Sun and Luk, 2017). The Z-B substrate has a 3xFLAG tag on the C terminus of H2B (Z-B$^F$) that slows the mobility of the nucleosome cumulatively as one or both untagged nucleosomal A-B dimers are replaced by Z-B$^F$ (Figures 1C and 1D) (Sun and Luk, 2017). The AA nucleosomal substrate is conjugated to the fluorescent molecules Cy3 or Alexa 647 on the 5' end on one strand of the nucleosomal DNA to facilitate in-gel fluorescence densitometry (Sun and Luk, 2017). When ASAP-purified SWR was incubated with AA nucleosomes, Z-B$^F$ dimers, and ATP, more ZZ product was generated in comparison to equimolar amounts of SWR prepared by our previous method, which involved FLAG affinity purification followed by glycerol gradient sedimentation (FLAG-IP/G-grad) (Figures 1D and 1E) (Luk et al., 2010), indicating that ASAP-purified SWR was more active than FLAG-IP/G-grad-purified SWR. (ASAP-purified SWR is referred to as SWR hereafter.)

To mimic the *in vivo* nucleosome substrate of SWR, which has an NFR on one side and a short linker on the other, the nucleosome substrate used in the *in vitro* reaction was assembled using a 204-bp DNA with the 147-bp Widom 601 positioning sequence located

near one end such that a "long" 50-bp linker and a "short" 7-bp linker flank the core particle (50-N-7) (Figure 2A) (Segal et al., 2006). Because of this asymmetry, the replacement of one of the two A-B dimers with Z-B$^F$ generates AZ and ZA isomers that are conformationally different due to the position of the FLAG tag in relation to the long linker (Figures 2B and 2C), and thus the AZ and ZA nucleosomes migrated as a doublet using native PAGE (Figure 2D, lanes 1–4) (Sun and Luk, 2017). By contrast, the AZ and ZA species migrated as a single band when a pseudo-symmetrical 6-N-7 substrate (core particle flanked by a 6-bp and a 7-bp linker) was used (Figure 2F, lanes 1–4) (Sun and Luk, 2017).

Being able to distinguish the AZ and ZA isomers provided an opportunity to determine whether the first inserted Z-B$^F$ dimer is selectively targeted to one side of the nucleosome. Furthermore, this distinction allowed us to differentiate which of the two tracking strands (i.e., at SHL+2 and SHL-2) is used to generate the AZ or ZA species (Figures 2B and 2C). Previous studies showed that SWR is restricted to exchange one of two A-B dimers with Z-B by disrupting the continuity of the tracking strand with a 2-nt gap on one face of the nucleosome (Figure S1B) (Ranjan et al., 2015). When a 2-nt gap was introduced into the tracking strand distal to the long linker (i.e., the NFR) of 50-N-7, the formation of the ZZ species was reduced, and only the top band of the AZ/ZA doublet accumulated (Figures 2D and 2E). Therefore, the tracking strand distal to the NFR is responsible for generating the bottom band of the doublet. This result was not sufficient, however, to determine which bands represent the AZ or ZA species.

## Asymmetric Recruitment of SWR to the NFR Does Not Restrict H2A.Z Insertion to One Side of the Nucleosome

Consistent with an earlier report that showed that SWR preferentially binds to nucleosomes with NFRs of at least 40 bp (Ranjan et al., 2013), SWR deposited Z-B$^F$ into 50-N-7 at a faster rate than 6-N-7 (compare Figure 2D to Figure 2F, lanes 1–4, and Figure 2E to Figure 2G, left panels). Based on a recent structural model of the SWR-nucleosome complex, recruitment of SWR to the NFR is expected to position the ATPase motor onto the NFR-distal tracking strand (i.e., on the opposite DNA gyre) (Figure S1B) (Willhoft et al., 2018), and thus one band of the AZ/ZA doublet should be conformationally favored. Therefore, it was surprising to see that the AZ and ZA intermediates observed for the 50-N-7 reaction were produced at similar rates (Figure 2D, lanes 2 and 3). To ensure that the reduced activity of SWR with 6-N-7 was not an artifact of the loss of enzyme activity, we performed a competition experiment. The 50-N-7 and 6-N-7 AA substrates were incubated with SWR, Z-B$^F$ dimer, and ATP in the same reaction. Again, formation of the ZZ species was faster for 50-N-7 than 6-N-7, and the AZ and ZA bands within the doublet of the 50-N-7 reactions exhibited similar intensity (Figure 2H). This observation confirms that SWR prefers binding to nucleosomes with linkers 40 bp compared to shorter linkers (Ranjan et al., 2013). However, once bound, SWR exhibits little bias as to which side it will insert the Z-B dimer, even when one linker is longer. This result provides a molecular explanation for how SWR can generate ZZ nucleosomes at the +1 position when the NFR is only on one side.

## Insertion of Each Z-B Dimer Requires Engagement of the Tracking Strand on the Same Face of the Nucleosome

The fact that the insertion of Z-B dimers is restricted to one side of the nucleosome when a 2-nt gap is present in the 50-N-7 nucleosomes enabled us to determine on which face of the nucleosome the dimer was inserted. To this end, we developed a site-directed radical cleavage approach to identify the location of the nascent Z-B dimer in relation to the tracking strand—the site of ATPase motor action (Figures S1A and S1B). The assay involved attaching a hydroxyl radical cutter via an engineered cysteine on the incoming Z-B dimer. By restricting Z-B insertion to one side of the gapped nucleosome, the question is whether the cut site is associated with the intact tracking strand on the same face or the opposite face of the nucleosome. Two positions on yeast H2A.Z, L19 and V83, were chosen for cysteine substitution based on their proximity to the nucleosomal DNA at SHL±4 and SHL±5.5, respectively (Figure S2A) (Suto et al., 2000). Recombinant L19C and V83C H2A.Z proteins purified from bacteria were individually refolded with FLAG-tagged H2B to make $Z^{L19C}$-$B^F$ and $Z^{V83C}$-$B^F$ dimers, respectively. The copper chelator o-phenanthroline (OP) was conjugated to the cysteine on the mutant H2A.Z via sulfhydryl chemistry (Brogaard et al., 2012). The conjugation efficiencies of OP to L19C and V83C dimers were monitored indirectly by labeling unreacted cysteines with maleimide-Alexa 647 and were 96% and 74%, respectively (Figures S2B and S2C). To evaluate whether the OP-labeled Z-$B^F$ dimers were active substrates of SWR, they were used in the histone exchange reactions (Figures S2D–S2G). SWR was able to insert the OP-labeled Z-$B^F$ dimers into intact nucleosomes (with or without a long linker), as indicated by the formation of the AZ/ZA and ZZ species (Figures S2D and S2E). SWR also inserted the OP-labeled Z-$B^F$ into gapped nucleosomes, producing predominantly one heterotypic species at efficiencies comparable to the unlabeled Z-$B^F$ (Figures S2F and S2G).

Hydroxyl radical cutting of the OP-conjugated AZ, ZA, and ZZ products was initiated by the addition of hydrogen peroxide and copper I (generated by reducing copper II with 3-mercaptopropionic acid) (Brogaard et al., 2012). Site-specific cleavage of the nucleosomal DNA was determined by denaturing PAGE and fluorescence scanning, which monitored the fluorophore-labeled single-stranded DNA (ssDNA). The 2 L19 residues on a ZZ nucleosome are predicted to be located 45 bp on opposite sides of the dyad (Figure 3A). Therefore, if the OP-labeled $Z^{L19C}$-$B^F$ dimer was inserted into 50-N-7 on the side proximal to the NFR (and to the fluorophore), then a 78-nt species was expected, whereas a 168-nt species was expected for the distal side (Figure 3A, highlighted in green). The ~78-nt and ~168-nt species were observed when the intact 50-N-7 substrate was used (Figure 3C, lane 3). Since the 2 V83C sites on the ZZ nucleosome are located farther away from the dyad, cleavage resulting from the OP-labeled $Z^{V83C}$-$B^F$ dimer is expected to release an ~64-nt species when inserted on the NFR-proximal side and an ~182-nt species when inserted on the NFR-distal side (Figure 3B). Again, both cleavage products were observed when the intact 50-N-7 substrate was used, proving that the cleavage is specific and depends upon the position of the cysteines (Figure 3C, lane 4). Note that ZZ nucleosomes contain two OP-labeled Z-$B^F$ dimers, and therefore the DNA is cut twice. Only the shorter cleavage product containing the Cy3 label can be detected, and the origin of this fragment can therefore come from either ZZ or ZA nucleosomes.

The disruptive 2-nt gap of the gapped 50-N-7 substrate was present on the "bottom" strand in Figures 3A and 3B (red arrow), while the Cy3 label (green dot) was present on the intact "top" complementary strand. Hence, the gap itself would not influence the mobility of the labeled ssDNA in denaturing PAGE. Insertion of the OP-labeled Z-B$^F$ on one side of the gapped 50-N-7 nucleosome generated predominantly the smaller cleavage product (~78 nt for L19C or ~64 nt for V83C), indicating that the undamaged tracking strand that allows Z-B dimer insertion is proximal to the NFR/Cy3 label (Figure 3C, lanes 7 and 8). Since some background bands overlapped with the regions where we expected to see the longer cleavage products, background subtraction was performed on the OP cleavage profiles of the nucleosomes inserted with the cysteine-labeled H2A.Z (Figure 3C, lanes 3 and 4 and 7 and 8) using the profile of the unmodified H2A.Z-containing nucleosomes as a normalization control (Figure 3C, lanes 2 and 6, respectively). The normalized Cy3 profiles demonstrated a decrease in the larger cleavage products (i.e., ~168 nt for L19C and ~182 nt for V83C) when the gapped 50-N-7 was used (Figure 3D), indicating that H2A.Z insertion is restricted to the face of the nucleosome, where the intact NFR-distal tracking strand is present.

A gapped version of the 6-N-7 substrate was also tested side by side with the intact 6-N-7 substrate (Figures 3E–3H). Consistent with the results for the gapped 50-N-7 substrate, the OP-induced cut sites occurred on the same side of the nucleosome with the intact tracking strand (Figures 3G, lanes 3 and 4 and 7 and 8, and 3H). This observation reinforces the idea that DNA translocation and the concomitant H2A.Z insertion occur on the same face of the nucleosome. A recent study that used fluorescence resonance energy transfer (FRET) to monitor SWR-mediated H2A.Z exchange independently arrived at the same conclusion (Singh et al., 2019).

## SWR Preferentially Inserts H2A.Z onto One Face of the Nucleosomal Substrate at Suboptimal Temperatures

To understand the mechanism of how SWR accesses both faces of an asymmetrically positioned nucleosome (50-N-7) to deposit H2A.Z, we focused on an unexpected result obtained serendipitously when a histone exchange reaction was allowed to proceed at 4°C overnight. In this reaction, SWR produced predominantly faster migrating AZ nucleosomes —the species expected when SWR acts on the conformationally "favored" NFR-distal tracking strand (Figure S3A).

At 30°C, the optimal growth temperature of budding yeast, SWR exhibited robust activity, as evidenced by a 50% depletion of the initial AA nucleosomes ($AA_{50}$) in ~10 min (Figures 4A and 4B, pink). The AZ and ZA intermediates accumulated to 50% of the initial AA nucleosomes ($AZ/ZA_{50}$) in ~15 min (Figures 4A and 4B, blue) and were chased into the ZZ product, which accumulated to 50% of the initial AA level ($ZZ_{50}$) in ~35 min (Figures 4A and 4B, green). When the AZ and ZA bands were quantified individually, both intermediates accumulated at similar initial rates (0.3 nM/min) (Figures 4A and 4B, red and black), consistent with SWR being able to access both tracking strands of the 50N-7 substrate efficiently under physiological temperature.

At lower temperatures, the overall rate of histone exchange decreased in a non-linear fashion. Notably, $AA_{50}$ increased to 13 min at 23°C, ~30 min at 16°C, 144 min at 10°C, and

195 min at 4°C (Figures 4A–4J, pink, and S3B), while $ZZ_{50}$ increased to 49 min at 23°C, 108 min at 16°C, and 1,020 min at 10°C (Figures 4A–4J, green, and S3C; $ZZ_{50}$ for 4°C was not determined as the reaction was too slow). In addition, decreasing temperatures disproportionately inhibited the formation of ZA nucleosomes (Figures 4C–4J, compare red and black lines). Since ZA formation requires the NFR-proximal tracking strand at SHL2 and AZ formation requires the NFR-distal tracking strand at SHL+2, decreasing temperature makes SWR progressively more biased against the NFR-proximal SHL-2 site.

The temperature-dependent phenomenon was similarly observed for the AZ-to-ZZ transition, which involves the insertion of a second Z-B dimer using the NFR-proximal tracking strand. This phenomenon was particularly evident in the 4°C reaction, which generated predominantly the AZ intermediate. The majority of AA nucleosomes (>95%) were converted to the AZ configuration after 10 h, but the AZ-to-ZZ transition took much longer (Figures 4I and 4J, pink). Only 19% of ZZ nucleosomes (relative to the AA input) were produced within the 10- to 24-h period (Figures 4I and 4J, green). Therefore, at suboptimal temperatures, the insertion of Z-B dimers at the NFR-proximal site is slow for this nucleosomal substrate regardless of whether it is the first or second H2A.Z-containing dimer.

At 37°C, SWR exhibits no preference for Z-B insertion on either side of the 50-N-7 substrate. However, the overall histone exchange rate decreased in comparison to the 30°C reaction ($AA_{50}$ >60 min; Figures 4K and 4L). The loss of activity associated with overheating is at least partially reversible, as a histone exchange reaction pre-incubated at 37°C before the addition of ATP at 23°C exhibited relatively robust activity (Figure S3D). Therefore, the loss of activity at 37°C is not caused by the irreversible deterioration of enzyme integrity.

## Linker DNA Twisting Is Not a Major Energy Barrier for SWR to Switch Sides

One possible explanation for the biased H2A.Z insertion at suboptimal temperatures is that NFR recruitment of SWR presents the NFR-distal tracking strand more naturally to the remodeling ATPase for NFR-distal insertion (Figure S4A). Higher temperatures increase linker DNA flexibility, allowing the nucleosome to swivel and present the NFR-proximal site for H2A.Z insertion, but lower temperatures exaggerate this bias. To test this hypothesis, 2-nt gaps were systematically introduced into the linker DNA on the NFR side of the nucleosome substrate (Figure S4A, purple region). If DNA twisting is a major energy barrier for NFR-proximal insertion, then the DNA gap is expected to facilitate nucleosome core swiveling with respect to the remodeling ATPase, and hence, Z-B insertion should become unbiased at suboptimal temperatures. Contrary to this expectation, strong NFR-distal insertion preference remained for 50-N-7 substrates with 2-nt gaps at positions [−7,−8], [−12,−13], [−15,−16], and [−17,−18] (where position 0 refers to the last nucleotide at the end of the nucleosomal DNA) under suboptimal temperatures (Figures S4B–S4D). We conclude that linker DNA twisting is not a major energy barrier for H2A.Z insertion on the NFR-proximal site.

## Nucleosomal DNA Sequence Plays a Major Role in Modulating SWR Remodeling Activity

The Bowman lab has shown that the sliding activity of another ATP-dependent remodeler, Chd1, is affected by nucleosomal DNA sequences (Winger and Bowman, 2017), raising the possibility that the biased H2A.Z insertion at the NFR-distal site is caused by the presence of a specific DNA element(s) in the asymmetric Widom sequence that stimulates histone exchange. If true, then flipping the Widom sequence relative to the NFR should make the new NFR-proximal site more favorable for H2A.Z insertion at suboptimal temperatures.

To test this hypothesis, nucleosomes reconstituted with the canonical or flipped Widom sequences (in relation to the NFR) (Figures 5A, 5D, and S5A) were incubated with SWR in the presence of OP-labeled $Z^{L19C}$-$B^F$ dimers and ATP at 30°C or 4°C. Time courses based on the radical cleavage assay were performed with Alexa 647-labeled nucleosomal substrates (which provide more robust densitometry signals than the Cy3-labeled substrates). At 30°C, the canonical Widom nucleosomes were cleaved on both sides with no major bias, as evidenced by ~50% NFR-proximal cutting (% Prox), which refers to the relative intensity of the NFR-proximal cleavage product (Prox) over total (i.e., NFR-distal [Dist] and Prox combined) (Figure 5B). The flipped nucleosomes were also cleaved on both sides at 30°C (Figure 5E), but at 4°C, insertion bias was increased for both the canonical and the flipped substrates, although in opposite directions. The canonical substrate was cut predominantly at the NFR-distal site (13% Prox at 4 h), while the flipped substrate was cut at the NFR-proximal site (86% Prox at 4 h) (Figures 5C and 5F). These results indicate that the DNA sequence on the NFR-distal half of the canonical sequence is stimulatory to SWR activity, while the NFR-proximal half is inhibitory. Suboptimal reaction temperatures exaggerated the differential effects of these sequences on H2A.Z insertion.

TA dinucleotides at the inward-facing minor grooves of a nucleosome, especially those that interact with H3-H4, are important in stabilizing nucleosomes (Chua et al., 2012; Segal et al., 2006). Since the NFR-distal side has fewer (H3-H4)-interacting TA dinucleotides, looser (H3-H4)-DNA contacts could facilitate the A-B dimer eviction and thus Z-B insertion. However, this possibility was ruled out as a Widom derivative called TA+2, in which 2 TA dinucleotides that were added back to the TA-deficient side at SHL+0.5 and SHL+2.5 (Figures 5G, orange arrows, and S5A, orange underlines) did not alter H2A.Z insertion bias as compared to the canonical Widom control at both 30°C and 4°C (compare Figures 5H and 5I to S5B and S5C).

The sequence composition of a 16-bp region that spans SHL2.5 and SHL3.5 plays a key role in modulating the sliding activity of Chd1 (Winger and Bowman, 2017). To test whether this is also true for SWR, nucleosomes were reconstituted with the SHL3-swap sequence, which interchanged two 16-bp regions around SHL3 on both halves of the canonical Widom sequence (Figures 5J and S5A). At 30°C, the SHL3-swap nucleosome was cut by OP-labeled Z-B dimers on both sides but with more robust cutting on the NFR-proximal side (79% Prox at 15 min) (Figure 5K), indicating that the substituted 16-bp region (TAGGGAGTA ATCCCCT) was stimulatory to H2A.Z insertion, whereas the corresponding region on the distal side (TCGTAGCAA GCTCTAG) was inhibitory (Figure S5A). The differential H2A.Z insertion activity was even more pronounced at 4°C (84% Prox at 4 h), recapitulating the cleavage pattern of the flipped nucleosome (Figures 5F and 5L).

To rule out that the accumulation of the smaller cleavage fragment in SHL3-swap was an artifact of double cutting by the ZZ product, time courses for the 30°C and 4°C reactions before hydroxyl radical cutting were analyzed by the nucleosome mobility assay. Preferential production of the ZA (NFR-proximal) over AZ (NFR-distal) species at both temperatures was still observed, which is consistent with preferential H2A.Z insertion on the NFR-proximal site (Figures S5B and S5C).

### G/C Runs Are Linked to Enhanced H2A.Z Insertion Activity *In Vivo*

SWR exhibited a stronger bias in depositing H2A.Z on the NFR-proximal side with the SHL3-swap substrate (79% Prox at 15 min) than with the flipped substrate (41% Prox at 15 min), even at 30°C (Figures 5E and 5K). This result was interesting because both substrates bear the 16-bp stimulatory sequence on the NFR-proximal side. This observation therefore suggests that other DNA elements on the NFR-proximal side of SHL3-swap act synergistically with the 16-bp region to promote H2A.Z insertion.

One possibility is that the presence of extra G/C runs ( 3 consecutive G or C nucleotides) on the NFR-proximal half of SHL3-swap, spanning between SHL4.5 and SHL6, further destabilizes the DNA contacts with the outgoing A-B dimer to assist in the eviction step of the histone exchange process (Travers and Klug, 1987) (Figure S5A, underscored in gray). Together with the G/C runs in the 16-bp stimulatory region, the DNA associated with the preferred outgoing A-B dimer of SHL3-swap has a disproportionately higher number of G/C runs than the corresponding region of the flipped nucleosome (Figure S5A). To test the hypothesis that the presence of G/C runs around the A-B dimer is linked to a more robust H2A.Z deposition activity, we turned to a genomic approach. DNA sequences underlying +1 nucleosomes were extracted from the yeast genome and ranked according to H2A.Z occupancy (Tramantano et al., 2016). The G/C-trinucleotide (SSS) frequencies of the most H2A.Z enriched +1 nucleosomes (top 25%) versus the least enriched (bottom 75%) were plotted along the dyad distance (Figure 6). Consistent with our hypothesis, a higher SSS frequency is observed in +1 nucleosomes with more H2A.Z. The strongest SSS enrichment sites are localized between SHL3.5 and SHL6 on both sides of the nucleosome, coinciding with the binding region of A-B dimers (Figure 6). The +1 nucleosomes with less H2A.Z are generally more depleted for SSS when compared to the full complement of annotated nucleosomes (Figure 6, compare blue and black). Our results are in agreement with the role of G/C runs in promoting H2A.Z insertion activity of the SWR complex.

## DISCUSSION

The SWR complex catalyzes a unique ATP-driven chromatin remodeling reaction in which two Z-B dimers sequentially replace the two A-B dimers in a canonical nucleosome to form a homotypic ZZ nucleosome (Luk et al., 2010). ZZ nucleosomes are enriched at the +1 positions of most promoters, more so than are the AZ/ZA species (Luk et al., 2010). The homotypic ZZ configuration appears to be the optimal chromatin state for transcription, as the transcription machinery preferentially targets +1 ZZ nucleosomes for disassembly (Mohan et al., 2018; Tramantano et al., 2016), and H2A.Z is required for a rapid, distinct transcriptional response (Cortijo et al., 2017; Dhillon et al., 2006; Zhang et al., 2005).

However, given that SWR is asymmetrically recruited to the NFR side on the +1 nucleosome, the question of how SWR accesses both faces of the nucleosome to generate a ZZ nucleosome was not fully understood.

This study presents two new lines of evidence that challenge the notion that an NFR-bound SWR complex would preferentially position the remodeling ATPase to act on the NFR-distal tracking strand of a +1 nucleosome and insert H2A.Z distal to the NFR (Ranjan et al., 2015; Rhee et al., 2014; Singh et al., 2019). First, at the optimal reaction temperature, SWR generates the AZ and ZA species at comparable rates, indicating that SWR (even when recruited by the NFR) can switch sides and easily access the NFR-proximal site (Figure 7A), which is consistent with a conclusion made by the Wigley group (Willhoft et al. (2018). A similar side-switching mechanism has also been observed for the chromatin remodeler Chd1 that allows bidirectional nucleosome sliding (Qiu et al., 2017). Second, the observed NFR-distal bias for H2A.Z insertion at suboptimal temperatures is mainly due to the asymmetrical sequence of the Widom DNA (Figure 7B, pink). SWR can in fact insert H2A.Z preferentially on the conformationally unfavorable NFR-proximal side when the stimulatory sequence is swapped to the NFR-proximal side (Figure S6, pink). Therefore, DNA sequences favorable for H2A.Z insertion dominate over any conformational bias. This observation is significant because many +1 nucleosomes in yeast (as shown by chromatin IP [ChIP]-exo conducted at 25°C) are more enriched for H2A.Z on the NFR-distal side (Rhee et al., 2014). The original interpretation was that the asymmetric recruitment of SWR causes NFR-distal insertion of H2A.Z; however, this work argues that nucleosomal DNA sequences could play a major role in directing H2A.Z onto the NFR-distal side. Rhee et al. (2014) also found that higher G/C content is associated with H2A.Z enrichment on the NFR-distal side of a major population of +1 nucleosomes and is thus consistent with our conclusion.

A recent study used single-molecule FRET to study SWR-mediated histone exchange on the Widom nucleosomes (at room temperature) and concluded, similar to the present study, that the asymmetric sequence on the two halves of the Widom sequence differentially affects H2A.Z insertion activity (Singh et al., 2019). We have extended this observation to show that the most critical region involved in stimulating (or inhibiting) the H2A.Z insertion activity of SWR is a 16-bp region located around SHL±3 (Figure 7C, dark pink), whereas another region contacting the outgoing A-B dimer is likely secondary (Figure 7C, light pink). A recent cryoelectron microscopy (cryo EM) structure of the SWR-bound nucleosome offers some clues as to why these regions are important. In the ATP-bound state, the ATPase motor of SWR lifts the DNA off the histones in and around SHL+2, distorting the duplex structure between SHL+2.5 and SHL+3.5, while the Swc6/Arp6 subunits unwrap 2.5 turns of DNA from the entry site (Willhoft et al., 2018) (Figure 7D). The stimulatory elements could be more susceptible to such distortion, whereas the inhibitory elements may require additional heat to overcome the energy barrier (Travers and Klug, 1987). Since artificial nucleosomal sequences were used in our remodeling assays, however, a more complex picture may emerge of how DNA sequence affects the activity of SWR as we interrogate the full complement of endogenous nucleosomal substrates. Notwithstanding the limitations of this study, the fact that the same region of the Widom sequence stimulates the sliding activity of another ATP-dependent remodeler Chd1 (which has no common subunit with SWR) points

to DNA translocation being the mechanistic step affected by the sequence (Winger and Bowman, 2017).

As substantial amounts of AZ and ZA species were detected during the course of histone exchange reactions (even when catalytic amounts of SWR were used), our data suggest that SWR inserts the two Z-B dimers into the same nucleosome in a non-processive, stochastic manner. A related question is whether AZ/ZA nucleosomes are a better or worse substrate than AA nucleosomes. At 30°C, the insertion rate of the first Z-B dimer is 0.6 nM/min, while the rate for the second is 0.24 nM/min (estimated based on the initial 10 min and final 27 min of the 30°C time course, representing the AA-to-AZ/ZA and AZ/ZA-to-ZZ steps, respectively) (Figures 4A and 4B). This observation is consistent with the AZ/ZA nucleosome being a poorer substrate, as it has one less A-B dimer available for exchange than the AA nucleosome. At 4°C, the second Z-B insertion (3 pM/min) was much slower than the first (46 pM/min) (Figures 4I and 4J). However, since the interface between H2A and H2A.Z or between themselves within the octameric histone core is rather flexible (Mohan et al., 2018), the slowness of the second insertion is unlikely a consequence of difference in structural compatibility of the AA, AZ/ZA, and ZZ configurations. Rather, we interpret the slow second insertion as a consequence of a more demanding A-B eviction step when the outgoing dimer is associated with a DNA sequence that is more difficult to remodel.

In conclusion, it is well established that the site-specific insertion of H2A.Z at +1 nucleosomes is contributed in part by the affinity of SWR to long nucleosome-free DNA and histone modifications associated with transcriptionally active promoter regions (Raisner et al., 2005; Ranjan et al., 2013). This study shows that DNA sequences underlying nucleosomes play a major role in regulating the H2A.Z insertion activity of SWR, suggesting that nucleosomes can be hard coded with genetic information that regulates the targeting of H2A.Z with sub-nucleosomal specificity. Given that the influence of nucleosomal DNA sequence on H2A.Z insertion is strongly influenced by temperature, this work reveals for the first time that the remodeling output of a chromatin-modifying enzyme could be tuned by environmental temperature. Future work will focus on deciphering the exact nature of the sequence that promotes or inhibits H2A.Z insertion and how the different H2A.Z nucleosome configurations modulate downstream molecular events such as transcription.

## STAR★METHODS

### LEAD CONTACT AND MATERIALS AVAILABILITY

Please contact Ed Luk (ed.luk@stonybrook.edu) for further information. All unique/stable reagents generated in this study are available from Dr. Luk with a completed Materials and Transfer Agreement.

### EXPERIMENTAL MODEL AND SUBJECT DETAILS

*Saccharomyces cerevisiae* strains used in this study are listed in the Key Resources Table. Recombinant DNAs for expression of histones are of *Saccharomyces cerevisiae* origin.

## METHOD DETAILS

**Yeast Strains**—The yeast strain used in the purification of SWR by ASAP bore the *SWR1-3xFLAG-loxP, RVB1-MBP-loxP*, and *htz1 ::kanMX* alleles and was derived from the W1588-4C genetic background (W303 *MATa RAD5*+). The strain was constructed by first integrating a *3xFLAG-loxP-kanMX-loxP* cassette into the 3' end of the *SWR1* locus using the one-step gene replacement procedure, followed by Cre/*loxP*-mediated removal of the *kanMX* cassette, generating the yeast strain yEL168 (W1588-4C *SWR1-3xFLAG-loxP*) (Güldener et al., 1996; Longtine et al., 1998). The *MBP-loxP-kanMX-loxP* cassette was similarly integrated into the 3' end of the *RVB1* locus in yEL168, followed by Cre/loxP-mediated removal of *kanMX* to generate yEL410 (W1588-4C *SWR1-3xFLAG-loxP RVB1-MBP-loxP*). Finally, *HTZ1* of yEL410 was replaced with *kanMX* by the one-step gene replacement approach. The resulting strain yEL427 (W1588-4C *SWR1-3xFLAG-loxP RVB1-MBP-loxP htz1 ::kanMX*) was used for SWR purification by the ASAP procedure. To purify SWR with the FLAG-IP/G-grad approach, the strain yEL190 (W1588-4C *SWR1-3xFLAG-loxP-kanMX-loxP htz1 ::natMX*) was used (Sun and Luk, 2017).

**Plasmids**—The pET28a-*HTZ1* (pEL350) vector for bacterial expression yeast Htz1 was made by subcloning the *HTZ1* gene fragment into pET28a via the NcoI and XhoI sites. The cysteine mutant variants pET28a-*htz1*(*L19C*) (pEL542) and pET28a-*htz1*(*V83C*) (pEL543) were generated from pEL350 using the QuikChange site-directed mutagenesis kit (*Agilent*) with primer pairs EL1103 and EL1104 for L19C and EL1105 and EL1106 for V83C. Sequence integrity of all plasmids was confirmed by Sanger Sequencing (*Genewiz*). The *pUC57-Widom-601-(c1)* plasmid (pEL550) was synthesized and subcloned by *GenScript*. Primer sequences are available in Table S1.

**Native Protein Purification**—To prepare SWR by the ASAP procedure, yEL427 cells were grown in $6 \times 2$ L yeast extract peptone dextrose (YPD) medium to an optimal density at 600 nm ($OD_{600}$) of ~4 before harvested by centrifugation. After washing the cell pellets once with water and once with buffer A [300 mM HEPES-KOH (pH 7.6), 40% glycerol, 2 mM EDTA, 100 mM KCl, plus $2\times$ protease inhibitors (PI; 0.34 mg/mL PMSF, 0.66 mg/mL benzamidine hydrochloride, 2.74 μg/mL pepstatin A, 0.56 μg/mL leupeptin, and 4 μg/mL chymostatin)], the packed-cell volume (PCV) was recorded. The cells were stirred into a paste using the residual buffer A and dripped into liquid nitrogen. The resulting yeast 'nuggets' were pulverized under liquid nitrogen in a Freezer Mill (SPEX) at 15 strokes per sec for $15 \times 1$-min cycles separated by 1-min pause intervals. When the lysate was about to thaw, two PCV of buffer B [150 mM HEPES-KOH (pH7.6), 20% glycerol, 1 mM EDTA, 50 mM KCl, and $1\times$ PI] was added. Protein extraction was performed by adding 0.2 M KCl and incubating at 4°C with gentle mixing for 30 min. Extracts were cleared by centrifugation at $83,000 \times g$ for 2 hr in a SW28 rotor and were then incubated with 10 mL of Amylose resin (*New England Biolabs*) for 1 hr at 4°C. The beads were washed 4 times with buffer C [25 mM HEPES (pH 7.6), 1 mM EDTA, 10% glycerol, 0.01% NP-40, 0.3 M NaCl, $1\times$ PI, 1 mM DTT]. Rvb1-MBP containing SWR and INO80 complexes were eluted with 2 3 5 mL Buffer D [Same as Buffer C, except that it has 10 mM maltose but no DTT] at 4°C. The combined eluate, which contained SWR, INO80, and R2TP, was subjected to anti-FLAG affinity purification for the FLAG-tagged SWR complex by incubating with 2 mL of anti-FLAG M2

agarose (*Sigma-Aldrich*) for 2 hr at 4°C. The agarose beads were washed 3 times with 12 mL of buffer E [Same as buffer C, except that DTT was omitted] and eluted with buffer F [25 mM HEPES pH 7.6, 1 mM EDTA, 30% Glycerol, 0.01% NP-40, 0.3M NaCl, 1× PI, 0.5 μg/μl 3× FLAG peptide (*Biopeptide*)] for 2 hr at 4°C. The FLAG eluate was further cleared by filtration using a 0.22 μm PVDF membrane (*EMD Millipore*) and was supplemented with 1 mM DTT before flash freezing and storing at −80°C.

**Recombinant Histones and Nucleosomes—**Recombinant *S. cerevisiae* histone genes and mutant variants were overexpressed in the *E. coli* strain BL21-CodonPlus(DE3)-RIL and the histones were purified and lyophilized according to Vary et al. (2004). Canonical histone octamers were reconstituted by first unfolding and mixing the individual histones in buffer G [7 M guanidinium-HCl, 20 mM Tris-HCl (pH 7.5), 10 mM DTT] followed by dialysis into the refolding buffer H [2 M NaCl, 10 mM Tris-HCl (pH 7.5), 1 mM EDTA, 5 mM beta-mercaptoenthanol, 0.2 mM PMSF] as described in Vary et al. (2004). The octamers were fractionated on a Superdex-200 prep grade (XK16/70) column to remove aggregates, histone tetramers, dimers, and monomers. Wild-type Z-B dimers and the cysteine-containing variants were reconstituted similarly, except that they were fractionated on a Superdex 200 Increase 10/300 GL column in buffer I [2 M NaCl, 10 mM Tris-HCl (pH 7.5), 1 mM EDTA]. All histone dimers were dialyzed against buffer J [50 mM NaCl, 10 mM Tris-HCl (pH7.5), 1 mM EDTA, 0.01% NP-40] and concentrated to ~5–20 μM on a 10 kD MWCO Amicon Ultra-4 column (*EMD Millipore*) according to the manufacturer protocol. For the cysteine-containing variants, 17.5 μM of TCEP was added to the storage buffer. All histone dimers were stored at −80°C.

The DNA sequence used to generate the Canonical Widom 50-N-7 nucleosome contains the 601 (c1) positioning sequence (Segal et al., 2006) and can be found in Table S3. Cy3-labeling was achieved at the PCR step, where Taq was used to amplify the 50-N-7 template in plasmid pEL550 with forward primer EL336 [5'-(Cy3) TCT TCA CAC CGA GTT CAT CCC TT-3'] and reverse primer EL338 [5'-TAC ATG CAC AGG ATG TAT ATA TCT GAC-3']. The Cy3-labeled 6-N-7 nucleosomal DNA was generated similarly except that the forward primer 5'-[Cy3] GCC GCC CTG GAG AAT CC-3' (EL849) was used. The Alexa647-labeled nucleosomal DNA was prepared by labeling an amino-modified forward primer EL1223, [5'-(5AmMC6)-TCT TCA CAC CGA GTT CAT CCC TT-3'] (*IDT*), with Alexa647 succinimidyl ester according to the manufacturer protocol (*Thermo Fisher*, A20006). After purification on a 1x TBE / 15% polyacrylamide gel, the oligo was used in combination with EL338 or EL1178 to prime PCR synthesis using templates containing the 'Canonical Widom', 'Flipped', 'SHL3-swap', and 'TA+2' sequences. PCR products were purified by standard phenol/chloroform extraction and ethanol/NaOAc precipitation. After resuspension in buffer K [same as buffer J, except that NaCl concentration was increased to 300 mM], the DNA fragments were purified on a Superdex 200 Increase column using buffer K as eluent.

Gapped DNA was generated by a strategy previously described (Ranjan et al., 2015). Briefly, at the location of an intended single-stranded DNA gap, two consecutive deoxyuridines were incorporated into the PCR product in the primer synthesis step using primers EL1177, EL1192-7 (*IDT*) (Table S1). The modified DNA species were purified by

gel filtration as above followed by treatment with the uracil-specific excision reagent USER (*New England Biolabs*) at 37°C overnight to generate a 2-nt gap at the location of the uracil residues. Completion of the excision reaction was monitored by a 6% polyacrylamide gel, as the gapped DNA migrates slower than the intact DNA. After phenol-chloroform extraction and ethanol/NaOAc precipitation, the DNA was purified again by gel filtration as described above and concentrated with a 10 kD MWCO Amicon Ultra-0.5 column (*EMD Millipore*).

Nucleosomes were reconstituted by salt dialysis as previously described (Vary et al., 2004). Briefly, 1:1 molar ratio of purified DNA and octamers were mixed in buffer L [2 M NaCl, 10 mM Tris-HCl (pH 7.5), 1 mM EDTA, 0.01% NP-40] followed by dialysis in buffer J (Vary et al., 2004). The nucleosomes were then purified by sedimentation through a 15%–40% sucrose gradient in buffer M [25 mM HEPES-KOH (pH 7.6), 0.5 mM EDTA, 0.01% NP-40] at 192 000 × g for 20 hr at 4°C using the SW-55.1 rotor. The fractions containing the nucleosomes were dialyzed against buffer J and stored at 4°C.

**Modifying Histones with OP**—The OP conjugation protocol was adapted from Henikoff et al. (2014). Specifically, cysteine-modified Z-B dimers (4 μM) were mixed with TCEP (40 μM), and OP (140 μM) in the sulfhydryl-reactive form, N-(1,10-phenanthroline-5-yl)iodoacetamide (*Biotium* #92015) and incubated at room temperature for 2 hr in the dark. Labeled dimers were purified from any free OP by filtration in the PD SpinTrap G-25 column (*GE Healthcare*) pre-equilibrated with buffer J. OP labeling efficiency of the dimers (~2 μM) was indirectly monitored by reaction with Alexa-647 $C_2$ maleimide (2 μM) for 2 hr at room temperature in buffer J followed SDS-PAGE analysis. In-gel fluorescence was detected by a Typhoon FLA 9500 imager and quantified by the ImageQuant software (*GE Healthcare*). The same gel was then stained by SYPRO Ruby to control for loading.

***In Vitro* Histone Exchange Assay**—Histone exchange reactions were performed as previously described with minor modifications (Sun and Luk, 2017). Each 25 μL reaction had three components: Part A, B, and C in 3:1:1 ratio. Part A was 4 nM ASAP-SWR in 25 mM HEPES-KOH (pH 7.6), 0.5 mM EGTA, 0.1 mM EDTA, 5 mM MgCl₂, 0.17 μg/μL BSA, 50 mM NaCl, 10% glycerol, 0.02% NP-40. Part B was 100 nM AA nucleosomes (with or without Cy3) and 575 nM Z-B dimers (with or without OP) in 10 mM Tris-HCl (pH 7.5) 1 mM EDTA, and 50 mM NaCl. Part C was 1 mM ATP and was added last to a mixture of Part A and Part B to initiate the reaction. After incubation under the indicated conditions, 2.3 ng/μL of lambda phage DNA (*New England Biolabs*) was added to quench the reaction. Five microliters of Nap1 at 3.5 μM in 70% (w/v) sucrose, 10 mM Tris-HCl (pH 7.8), 1 mM EDTA was mixed with the reaction immediately before 5–7 μL was analyzed by a 6% PAGE. Nap1 was necessary to prevent non-specific interactions between free histones and nucleosomal DNA (Sun and Luk, 2017).

**Radical Cleavage Assay**—Radical cleavage mapping of OP-labeled Z-B dimers on nucleosomes was performed based on a procedure described in Brogaard et al. (2012). After the histone exchange reaction was quenched by lambda phage DNA, 150 μM CuCl₂, 50 mM Tris-HCl (pH 7.5), 6 mM 3-mercaptopropionic acid (MPA) and 6 mM $H_2O_2$ were added in the order as listed. Cleavage reactions were allowed to proceed in the dark for 60 min at room temperature. For the reactions in Figure 3 (where Cy3-labeled substrates were used),

an ethanol precipitation step was used to concentrate the DNA. This was achieved by mixing 25 μL of the cleavage reaction with 75 μL of buffer N [10 mM Tris-HCL (pH 7.5), 1 mM EDTA], 10 μL 3 M sodium acetate (pH 5.2), and 275 μL ethanol followed by centrifugation at 20,400 ×g for 15 min. After washing with ethanol, the dried pellet was resuspended in 8 μl of buffer O (95% formamide, 0.02% SDS, 1 mM EDTA) plus 2 μl of a competitor DNA cocktail (25 μM of each of four oligos) (Tables S1 and S2). The competitor DNA fragments (with the same sequence as the labeled strand) were critical for preventing the labeled DNA from reannealing. For the cleavage reactions in Figure 5 (where Alexa647-labeled substrates were used), the ethanol precipitation step was omitted. Each reaction (4 μL) was mixed with 1 μL of the appropriate competitor DNA and 2 μL of buffer O. The DNA samples were heated at 95°C for 10 min and quickly cooled to 4°C in an ice/water bath before separation on an 8 M urea / 0.5× TBE / 6% PAGE gel in the Novex 1.5-mm mini gel system (*Life Technology*).

## QUANTIFICATION AND STATISTICAL ANALYSIS

Fluorescence densitometry was performed on a Typhoon 9500 scanner using the 1D Gel Analysis module of the ImageQuant TL 7.0 software package. Relative levels of AA, AZ, ZA, and ZZ species in Figures 1D, 2D, 2F, 4A, 4C, 4E, 4G, 4I, and 4K were determined using the Lane Profiles function with lane width set at 60% to measure fluorescence along the center of each lane to avoid the sides where nucleosome bands were smeary. Background subtraction was performed using the 'rolling ball' method (with maximal diameter) to determine baseline. Band intensities represent areas under peaks. Relative nucleosomal levels were normalized to the AA species at time zero.

The G/C trinucleotide (SSS) frequency in Figure 6 was calculated as follows. H2A.Z occupancy data of the yeast strain yEL154 (untreated) in Tramantano et al. (2016) were used to rank +1 nucleosomes previously annotated by Rhee et al. (2014), generating a ranked BED file. The sequences of the +1 nucleosomes were then extracted using the *getfasta* (with –name and –tab options) command in *BedTools*, generating a two-column, tab-delimited list with 4738 nucleosomal sequences. A python script, Nucleotide_pattern_tri_CG_v3.py (Data S1), was used to identify G/C-trinucleotide patterns (SSS, i.e., CCC, GGG, CCG, GGC, CGG, GCC, CGC, and GCG). If true, the position is marked as 1, if not as zero. The list of SSS scores was split into two to represent the top 25% most H2A.Z-enriched +1 nucleosomes and the bottom 75%. The sum of SSS patterns was calculated for each nucleotide position from the nucleosomal dyad and plotted as frequency of occurrence. The chromosome-wide frequency of SSS patterns was calculated similarly but with an unsorted yeast nucleosome list from Jiang and Pugh (2009) representing 61025 nucleosomes. A 3-nt moving window was applied to average the data in Figure 6.

## Supplementary Material

Refer to Web version on PubMed Central for supplementary material.

## ACKNOWLEDGMENTS

## REFERENCES

Albert I, Mavrich TN, Tomsho LP, Qi J, Zanton SJ, Schuster SC, and Pugh BF (2007). Translational and rotational settings of H2A.Z nucleosomes across the Saccharomyces cerevisiae genome. Nature 446, 572–576. [PubMed: 17392789]

Bartholomew B. (2014). Regulating the chromatin landscape: structural and mechanistic perspectives. Annu. Rev. Biochem. 83, 671–696. [PubMed: 24606138]

Brogaard KR, Xi L, Wang J-P, and Widom J. (2012). A chemical approach to mapping nucleosomes at base pair resolution in yeast. Methods Enzymol. 513, 315–334. [PubMed: 22929776]

Chua EYD, Vasudevan D, Davey GE, Wu B, and Davey CA (2012). The mechanics behind DNA sequence-dependent properties of the nucleosome. Nucleic Acids Res. 40, 6338–6352. [PubMed: 22453276]

Cortijo S, Charoensawan V, Brestovitsky A, Buning R, Ravarani C, Rhodes D, van Noort J, Jaeger KE, and Wigge PA (2017). Transcriptional regulation of the ambient temperature response by H2A.Z nucleosomes and HSF1 transcription factors in Arabidopsis. Mol. Plant 10, 1258–1273. [PubMed: 28893714]

Dechassa ML, Zhang B, Horowitz-Scherer R, Persinger J, Woodcock CL, Peterson CL, and Bartholomew B. (2008). Architecture of the SWI/ SNF-nucleosome complex. Mol. Cell. Biol. 28, 6010–6021. [PubMed: 18644858]

Dechassa ML, Sabri A, Pondugula S, Kassabov SR, Chatterjee N, Kladde MP, and Bartholomew B. (2010). SWI/SNF has intrinsic nucleosome disassembly activity that is dependent on adjacent nucleosomes. Mol. Cell 38, 590–602. [PubMed: 20513433]

Deindl S, Hwang WL, Hota SK, Blosser TR, Prasad P, Bartholomew B, and Zhuang X. (2013). ISWI remodelers slide nucleosomes with coordinated multi-base-pair entry steps and single-base-pair exit steps. Cell 152, 442–452. [PubMed: 23374341]

Dhillon N, Oki M, Szyjka SJ, Aparicio OM, and Kamakaka RT (2006). H2A.Z functions to regulate progression through the cell cycle. Mol. Cell. Biol. 26, 489–501. [PubMed: 16382141]

Flaus A, Martin DMA, Barton GJ, and Owen-Hughes T. (2006). Identification of multiple distinct Snf2 subfamilies with conserved structural motifs. Nucleic Acids Res. 34, 2887–2905. [PubMed: 16738128]

Goddard TD, Huang CC, Meng EC, Pettersen EF, Couch GS, Morris JH, and Ferrin TE (2018). UCSF ChimeraX: meeting modern challenges in visualization and analysis. Protein Sci. 27, 14–25. [PubMed: 28710774]

Güldener U, Heck S, Fielder T, Beinhauer J, and Hegemann JH (1996). A new efficient gene disruption cassette for repeated use in budding yeast. Nucleic Acids Res. 24, 2519–2524. [PubMed: 8692690]

Henikoff S, Ramachandran S, Krassovsky K, Bryson TD, Codomo CA, Brogaard K, Widom J, Wang J-P, and Henikoff JG (2014). The budding yeast Centromere DNA Element II wraps a stable Cse4 hemisome in either orientation in vivo. eLife 3, e01861.

Hong J, Feng H, Wang F, Ranjan A, Chen J, Jiang J, Ghirlando R, Xiao TS, Wu C, and Bai Y. (2014). The catalytic subunit of the SWR1 remodeler is a histone chaperone for the H2A.Z-H2B dimer. Mol. Cell 53, 498–505. [PubMed: 24507717]

Jiang C, and Pugh BF (2009). A compiled and systematic reference map of nucleosome positions across the Saccharomyces cerevisiae genome. Genome Biol. 10, R109. [PubMed: 19814794]

Kobor MS, Venkatasubrahmanyam S, Meneghini MD, Gin JW, Jennings JL, Link AJ, Madhani HD, and Rine J. (2004). A protein complex containing the conserved Swi2/Snf2-related ATPase Swr1p deposits histone variant H2A.Z into euchromatin. PLoS Biol. 2, E131.

Kornberg RD, and Lorch Y. (1999). Twenty-five years of the nucleosome, fundamental particle of the eukaryote chromosome. Cell 98, 285–294. [PubMed: 10458604]

Krietenstein N, Wal M, Watanabe S, Park B, Peterson CL, Pugh BF, and Korber P. (2016). Genomic nucleosome organization reconstituted with pure proteins. Cell 167, 709–721.e12.

Krogan NJ, Keogh M-C, Datta N, Sawa C, Ryan OW, Ding H, Haw RA, Pootoolal J, Tong A, Canadien V, et al. (2003). A Snf2 family ATPase complex required for recruitment of the histone H2A variant Htz1. Mol. Cell 12, 1565–1576. [PubMed: 14690608]

Liang X, Shan S, Pan L, Zhao J, Ranjan A, Wang F, Zhang Z, Huang Y, Feng H, Wei D, et al. (2016). Structural basis of H2A.Z recognition by SRCAP chromatin-remodeling subunit YL1. Nat. Struct. Mol. Biol. 23, 317–323. [PubMed: 26974124]

Longtine MS, McKenzie A 3rd, Demarini DJ, Shah NG, Wach A, Brachat A, Philippsen P, and Pringle JR (1998). Additional modules for versatile and economical PCR-based gene deletion and modification in Saccharomyces cerevisiae. Yeast 14, 953–961. [PubMed: 9717241]

Lorch Y, Maier-Davis B, and Kornberg RD (2006). Chromatin remodeling by nucleosome disassembly in vitro. Proc. Natl. Acad. Sci. USA 103, 3090–3093. [PubMed: 16492771]

Lorch Y, Maier-Davis B, and Kornberg RD (2014). Role of DNA sequence in chromatin remodeling and the formation of nucleosome-free regions. Genes Dev. 28, 2492–2497. [PubMed: 25403179]

Luger K, Mäder AW, Richmond RK, Sargent DF, and Richmond TJ (1997). Crystal structure of the nucleosome core particle at 2.8 A resolution. Nature 389, 251–260. [PubMed: 9305837]

Luk E, Ranjan A, Fitzgerald PC, Mizuguchi G, Huang Y, Wei D, and Wu C. (2010). Stepwise histone replacement by SWR1 requires dual activation with histone H2A.Z and canonical nucleosome. Cell 143, 725–736. [PubMed: 21111233]

Mattiroli F, Bhattacharyya S, Dyer PN, White AE, Sandman K, Burkhart BW, Byrne KR, Lee T, Ahn NG, Santangelo TJ, et al. (2017). Structure of histone-based chromatin in Archaea. Science 357, 609–612. [PubMed: 28798133]

Mizuguchi G, Shen X, Landry J, Wu W-H, Sen S, and Wu C. (2004). ATP-driven exchange of histone H2AZ variant catalyzed by SWR1 chromatin remodeling complex. Science 303, 343–348. [PubMed: 14645854]

Mohan C, Kim LM, Hollar N, Li T, Paulissen E, Leung CT, and Luk E. (2018). VivosX, a disulfide crosslinking method to capture site-specific, protein-protein interactions in yeast and human cells. eLife 7, e36654.

Nguyen VQ, Ranjan A, Stengel F, Wei D, Aebersold R, Wu C, and Leschziner AE (2013). Molecular architecture of the ATP-dependent chromatin-remodeling complex SWR1. Cell 154, 1220–1231. [PubMed: 24034246]

Nodelman IM, Bleichert F, Patel A, Ren R, Horvath KC, Berger JM, and Bowman GD (2017). Interdomain communication of the Chd1 chromatin remodeler across the DNA gyres of the nucleosome. Mol. Cell 65, 447–459.e6.

Qiu Y, Levendosky RF, Chakravarthy S, Patel A, Bowman GD, and Myong S. (2017). The Chd1 chromatin remodeler shifts nucleosomal DNA bidirectionally as a monomer. Mol. Cell 68, 76–88.e6.

Raisner RM, Hartley PD, Meneghini MD, Bao MZ, Liu CL, Schreiber SL, Rando OJ, and Madhani HD (2005). Histone variant H2A.Z marks the 5' ends of both active and inactive genes in euchromatin. Cell 123, 233–248. [PubMed: 16239142]

Ranjan A, Mizuguchi G, FitzGerald PC, Wei D, Wang F, Huang Y, Luk E, Woodcock CL, and Wu C. (2013). Nucleosome-free region dominates histone acetylation in targeting SWR1 to promoters for H2A.Z replacement. Cell 154, 1232–1245. [PubMed: 24034247]

Ranjan A, Wang F, Mizuguchi G, Wei D, Huang Y, and Wu C. (2015). H2A histone-fold and DNA elements in nucleosome activate SWR1-mediated H2A.Z replacement in budding yeast. eLife 4, e06845.

Rhee HS, Bataille AR, Zhang L, and Pugh BF (2014). Subnucleosomal structures and nucleosome asymmetry across a genome. Cell 159, 1377–1388. [PubMed: 25480300]

Rigaut G, Shevchenko A, Rutz B, Wilm M, Mann M, and Sé raphin, B. (1999). A generic protein purification method for protein complex characterization and proteome exploration. Nat. Biotechnol. 17, 1030–1032. [PubMed: 10504710]

Rivera-Calzada A, Pal M, Muñoz-Hernández H, Luque-Ortega JR, Gil-Carton D, Degliesposti G, Skehel JM, Prodromou C, Pearl LH, and Llorca O. (2017). The structure of the R2TP complex defines a platform for recruiting diverse client proteins to the HSP90 molecular chaperone system. Structure 25, 1145–1152.e4.

Saha A, Wittmeyer J, and Cairns BR (2005). Chromatin remodeling through directional DNA translocation from an internal nucleosomal site. Nat. Struct. Mol. Biol. 12, 747–755. [PubMed: 16086025]

Schwanbeck R, Xiao H, and Wu C. (2004). Spatial contacts and nucleosome step movements induced by the NURF chromatin remodeling complex. J. Biol. Chem. 279, 39933–39941.

Segal E, Fondufe-Mittendorf Y, Chen L, Thåstroöm A, Field Y, Moore IK, Wang J-PZ, and Widom J. (2006). A genomic code for nucleosome positioning. Nature 442, 772–778. [PubMed: 16862119]

Shen X, Ranallo R, Choi E, and Wu C. (2003). Involvement of actin-related proteins in ATP-dependent chromatin remodeling. Mol. Cell 12, 147–155. [PubMed: 12887900]

Singh RK, Fan J, Gioacchini N, Watanabe S, Bilsel O, and Peterson CL (2019). Transient Kinetic Analysis of SWR1C-Catalyzed H2A.Z Deposition Unravels the Impact of Nucleosome Dynamics and the Asymmetry of Histone Exchange. Cell Rep. 27, 374–386.e4.

Sinha KK, Gross JD, and Narlikar GJ (2017). Distortion of histone octamer core promotes nucleosome mobilization by a chromatin remodeler. Science 355, eaaa3761.

Sun L, and Luk E. (2017). Dual function of Swc5 in SWR remodeling ATPase activation and histone H2A eviction. Nucleic Acids Res. 45, 9931–9946. [PubMed: 28973436]

Suto RK, Clarkson MJ, Tremethick DJ, and Luger K. (2000). Crystal structure of a nucleosome core particle containing the variant histone H2A.Z. Nat. Struct. Biol. 7, 1121–1124. [PubMed: 11101893]

Telmer PG, and Shilton BH (2003). Insights into the conformational equilibria of maltose-binding protein by analysis of high affinity mutants. J. Biol. Chem. 278, 34555–34567.

Tramantano M, Sun L, Au C, Labuz D, Liu Z, Chou M, Shen C, and Luk E. (2016). Constitutive turnover of histone H2A.Z at yeast promoters requires the preinitiation complex. eLife 5, e14243.

Travers AA, and Klug A. (1987). The bending of DNA in nucleosomes and its wider implications. Philos. Trans. R. Soc. Lond. B Biol. Sci. 317, 537–561. [PubMed: 2894688]

Vary JC Jr., Fazzio TG, and Tsukiyama T. (2004). Assembly of yeast chromatin using ISWI complexes. Methods Enzymol. 375, 88–102. [PubMed: 14870661]

Willhoft O, Ghoneim M, Lin C-L, Chua EYD, Wilkinson M, Chaban Y, Ayala R, McCormack EA, Ocloo L, Rueda DS, et al. (2018). Structure and dynamics of the yeast SWR1-nucleosome complex. Science 362, eaat7716.

Winger J, and Bowman GD (2017). The sequence of nucleosomal DNA modulates sliding by the Chd1 chromatin remodeler. J. Mol. Biol. 429, 808–822. [PubMed: 28189426]

Yen K, Vinayachandran V, and Pugh BF (2013). SWR-C and INO80 chromatin remodelers recognize nucleosome-free regions near +1 nucleosomes. Cell 154, 1246–1256. [PubMed: 24034248]

Yuan G-C, Liu Y-J, Dion MF, Slack MD, Wu LF, Altschuler SJ, and Rando OJ (2005). Genome-scale identification of nucleosome positions in S. cerevisiae. Science 309, 626–630. [PubMed: 15961632]

Zhang H, Roberts DN, and Cairns BR (2005). Genome-wide dynamics of Htz1, a histone H2A variant that poises repressed/basal promoters for activation through histone loss. Cell 123, 219–231. [PubMed: 16239141]

Zhou CY, Johnson SL, Gamarra NI, and Narlikar GJ (2016). Mechanisms of ATP-Dependent Chromatin Remodeling Motors. Annu. Rev. Biophys. 45, 153–181. [PubMed: 27391925]

Zofall M, Persinger J, Kassabov SR, and Bartholomew B. (2006). Chromatin remodeling by ISW2 and SWI/SNF requires DNA translocation inside the nucleosome. Nat. Struct. Mol. Biol. 13, 339–346. [PubMed: 16518397]

**Highlights**

- The SWR chromatin remodeler engages stochastically on either side of a +1 nucleosome

- Temperature determines whether SWR inserts H2A.Z preferentially on one side of the nucleosome

- The sequence of a 16-bp region affects temperature-dependent H2A.Z insertion

- Nucleosomes with consecutive G/C bases are more H2A.Z enriched at yeast promoters
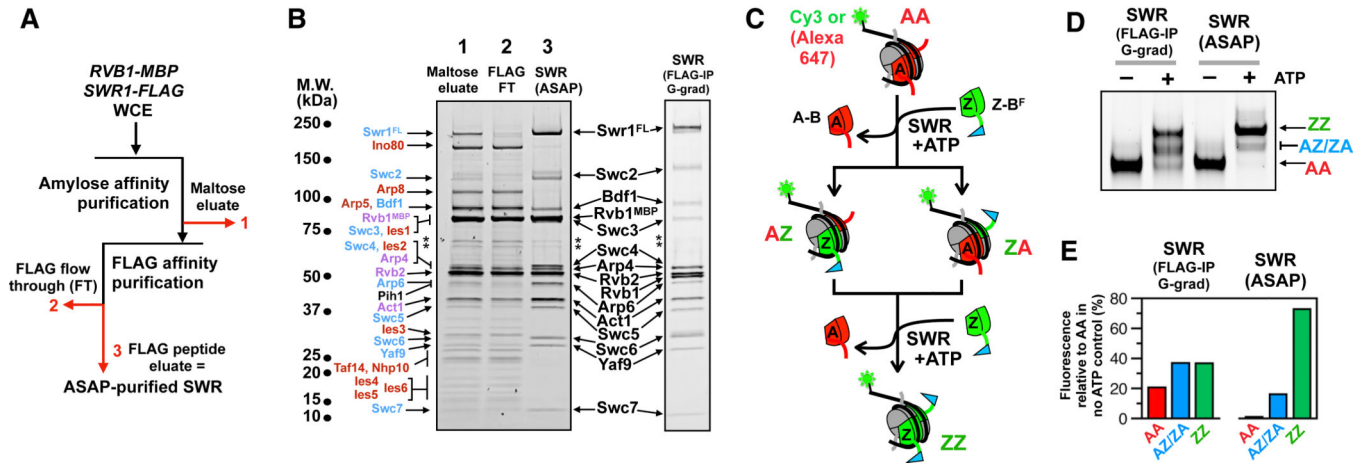
**Figure 1. ASAP-Purified SWR Exhibited Robust Remodeling Activity**

(A) The ASAP approach. Red numbers: samples analyzed in (B). WCE, whole-cell extracts.

(B) SDS-PAGE and SYPRO Ruby staining of the samples in (A). Red: unique to INO80. Blue: unique to SWR. Purple: shared between INO80 and SWR. Pih1 is a subunit of R2TP. Black: SWR components purified by ASAP and the FLAG-IP/G-grad approach. Asterisks: unknown factors co-purified with SWR.

(C) The histone exchange assay. Red: A-B dimers. Green: Z-B dimers. Blue flag: 3xFLAG tag on H2B. Green dots: fluorescent labels on the DNA.

(D) Native PAGE analysis to monitor histone exchange. SWR (2.4 nM) was mixed with 15 nM AA nucleosome and 115 nM H2A.Z-H2B$^{FL}$ with (+) and without (−) 200 μM ATP for 1 h at room temperature. The gel was scanned for Cy3 fluorescence.

(E) Quantification of the AA, AZ/ZA, and ZZ bands in the +ATP lanes relative to the AA band in the no-ATP controls.
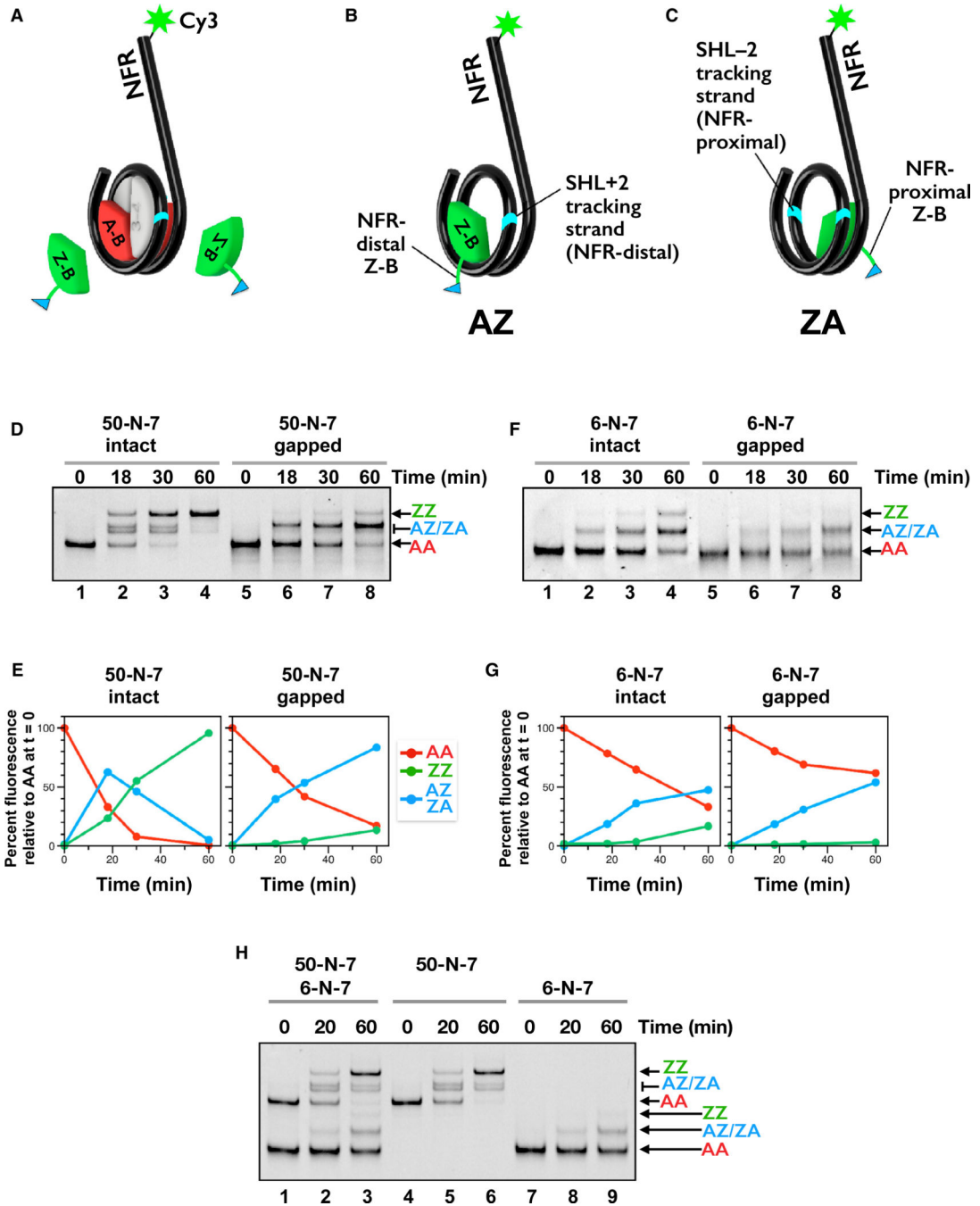
**Figure 2. A Gel-Based Assay for Monitoring SWR-Mediated H2A.Z Insertion**

(A) The 50-N-7 nucleosomal substrate used in the histone exchange reaction. Cyan: tracking strands.

(B) The Z-B dimer is distal to the NFR in the AZ nucleosome.

(C) Z-B is proximal to the NFR in ZA.

(D) Histone exchange reactions were performed as described in Figure 1D, except that 20 nM of 50-N-7 nucleosome was used instead of 15 nM.

(E) Quantification of (D).

(F) Same as (D), except that 6-N-7 nucleosomes were used.

(G) Quantification of (F).

(H) Same as (D), except that equimolar of canonical 50-N-7 and 6-N-7 nucleosomes were analyzed in combination (lanes 1–3) or separately (lanes 4–9). For the gapped nucleosomal substrates, the 2-nt DNA gap is located in the tracking strand on the NFR-distal side 19–20 nt from the dyad.
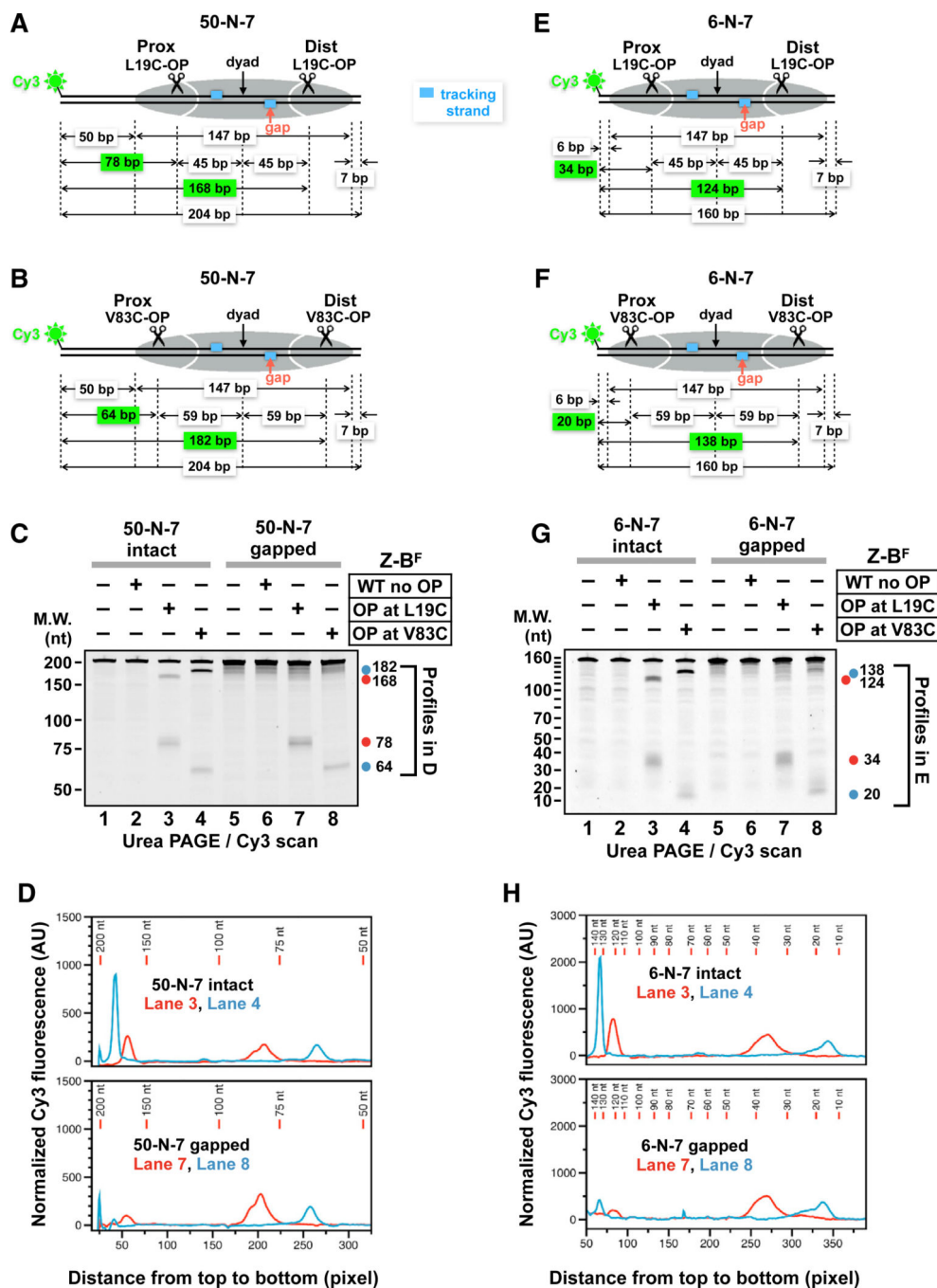
**Figure 3. SWR Inserts a Z-B Dimer on the Face of the Nucleosome with an Intact Tracking Strand**

(A and B) Diagrams representing the predicted cleavage sites on the 50-N-7 nucleosomes by OP at H2A.Z L19C in (A) or V83C in (B). The numbers in the green boxes indicate the expected sizes of the labeled cleavage products.

(C) OP-directed cleavage products were resolved by 8 M urea PAGE and detected by fluorescence scanning.

(D) Quantification of the profiles within the bracketed regions in (C). Lanes 3 and 4 were normalized to lane 2. Lanes 7 and 8 were normalized to lane 6. (E and F) Predicted cleavage sites of 6-N-7 by L19COP (E) and V83C-OP (F).

(G) Cleavage products of the 6-N-7 nucleosomes.

(H) Quantification of the profiles in (G) was performed as described in (D). Prox and Dist: proximal and distal to the NFR, respectively. Aliquots of the same histone exchange reactions from Figures S3C– S3F, lanes 6 and 8, were analyzed by radical cleavage here. The approximate ratios for AZ/ZA to ZZ were 6:4 and 7:3 for L19C and V83C, respectively.
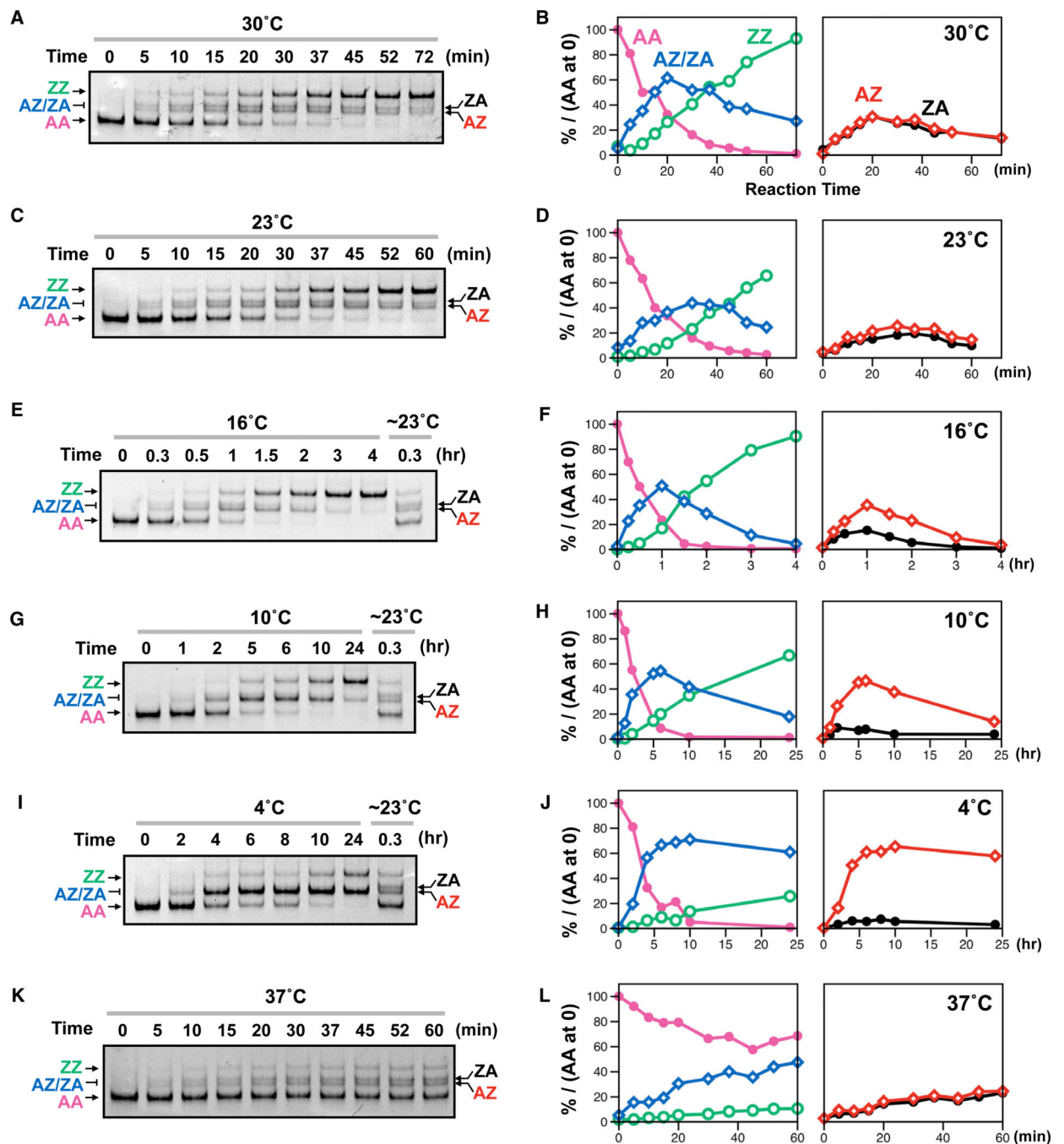
**Figure 4. Effects of Temperature on the Remodeling Activity of SWR**

(A) SWR was incubated with 50-N-7 nucleosomes and Z-B$^F$ dimers, as described in Figure 2, but at 30°C, which is the optimal growth temperature for *Saccharomyces cerevisiae*. The reaction was quenched by the addition of free DNA at the indicated time.

(B) Left: quantification of AA (pink), AZ/ZA (blue), and ZZ (green) of the reaction in (A). Right: AZ (red) and ZA (black) were quantified separately.

(C, E, G, I, and K) Same as (A), except that the reactions were performed under the indicated temperatures. The right lane of each experiment was a partial reaction conducted at room temperature, serving as markers for the different nucleosomal configurations.

(D, F, H, J, and L) Quantifications of the corresponding gels at left.
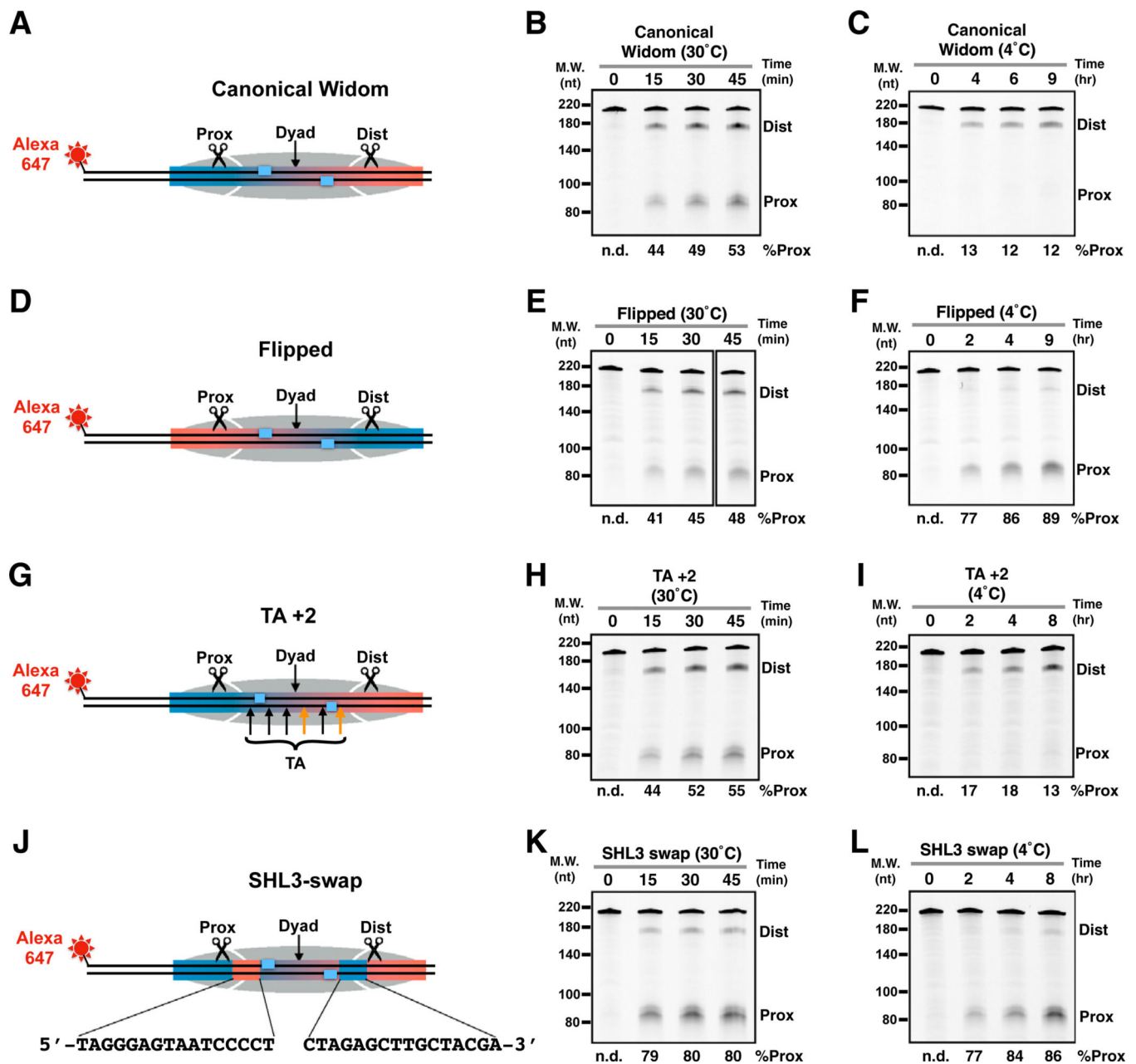
**Figure 5. The Role of Nucleosomal DNA Sequence in Sub-nucleosomal H2A.Z Targeting**

(A) A schematic representation of a 50-N-7 nucleosome with a canonical Widom sequence positioned in the same orientation as Figure 3A and an Alexa 647 fluorophore at the 5' end on the NFR side. Scissors represent the NFR-distal (Dist) and NFR-proximal (Prox) cut sites expected for insertion of a Z-B$^F$ dimer conjugated to OP at L19C. Blue boxes: ATPase tracking strands. Gray ovals: histone octamer position. Blue and red bars: blue represents the side where the H2A.Z insertion site is more sensitive to low temperature.

(B and C) Histone exchange time courses were conducted at 30°C or 4°C followed by radical cleavage and denaturing PAGE, as described in Figure 3. % Prox: relative amounts of NFR-proximal cleavage products (Prox) over total (i.e., Dist + Prox).

(D) The Widom sequence was flipped as compared to (A).

(G) Two additional minor groove TA anchors were added at the sites indicated by the orange arrows.

(J) Two 16-bp regions of the Widom sequence around SHL±3 were swapped.
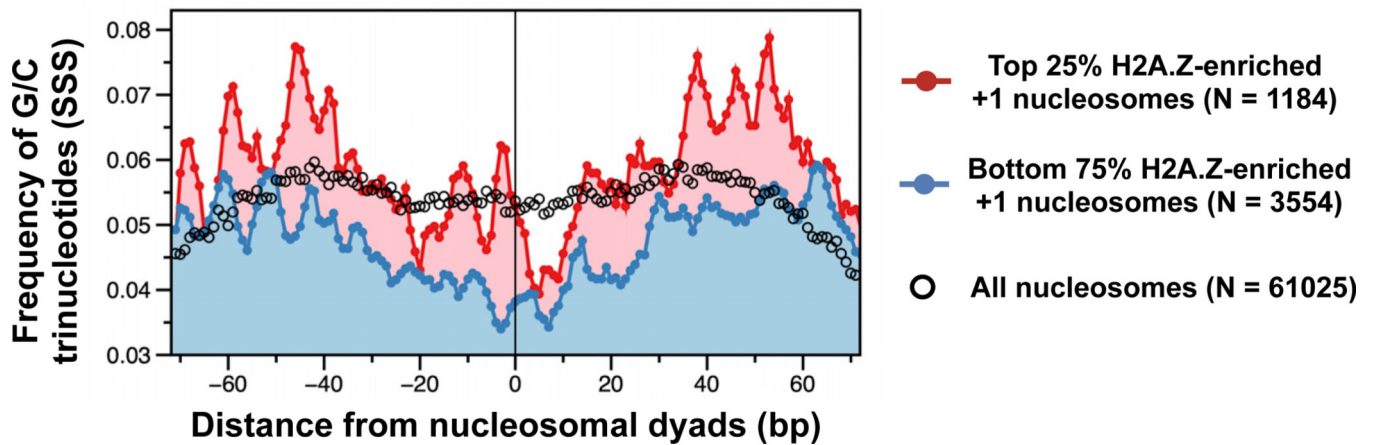
**Figure 6. G/C Runs Are Associated with H2A.Z-Enriched +1 Nucleosomes in Yeast**
The +1 nucleosomes (N = 4,738) of yeast were separated into 2 groups: the top 25% more H2A.Z enriched (red) versus the bottom 75% (bottom). The full complement of yeast nucleosomes was plotted as represented by the black open circles. The frequencies of G/C trinucleotides (3-nt moving average) were plotted along the nucleosomal DNA sequence centered at their dyads.

**Figure 7. Molecular Basis of the Temperature-Dependent Remodeling Activity of SWR**

(A)NFR-recruitedSWRaccessesbothsidesofthe+1nucleosomestochastically. Yellow arch and ovals: the SWR complex, highlighting only the Swr1 ATPase and the Swc2 subunit. White arrow: direction of ATPase motor action. Red and green arrows: movements of A-B (red) and Z-B (green) dimers. Gold: ATPase tracking strand. Pink: stimulatory sequence. Cyan: inhibitory sequence.

(B) At suboptimal temperatures, Swr1 ATPase encounters a stronger energy barrier on the side linked to the inhibitory sequence (cyan). Therefore, H2A.Z is preferentially inserted on the NFR-distal side in the first round of histone exchange. This insertion bias is exaggerated by decreasing the reaction temperature.

(C and D) DNA elements critical for H2A.Z insertion are highlighted pink (primary) and light pink (secondary) in 1KX5 (C, nucleosome alone) and in 6GEN (D, nucleosome with SWR). Gold: ATPase tracking strands. Orange: SWR components.

## KEY RESOURCES TABLE

| REAGENT or RESOURCE | SOURCE | IDENTIFIER |
|---|---|---|
| **Bacterial and Virus Strains** | | |
| *E.coli* strain BL21-CodonPlus(DE3)-RIL | Agilent | Cat# 230245 |
| **Chemicals, Peptides, and Recombinant Proteins** | | |
| 2-mercaptoethanol | Thermo Fisher | Cat# BP176-100 |
| 3-mercaptopropionic (MPA) | Millipore Sigma | Cat# M5801-100G |
| 3x FLAG peptide | Millipore Sigma | Cat# F4799-25MG |
| Adenosine 5'-triphosphate (ATP) | GE Healthcare | Cat# 272056 |
| Alexa-647 C$_2$ maleimide | Thermo Fisher | Cat# A20347 |
| Alexa-647 succinimidyl ester | Thermo Fisher | Cat# A20006 |
| Amylose Resin High Flow | NEB | Cat# E8022s |
| Anti-FLAG M2 Affinity Gel | Millipore Sigma | Cat# A2220 |
| Benzamidine hydrochloride | Millipore Sigma | Cat# B6506-100G |
| Bovine Serum Albumin (BSA) | Roche | Cat# 10-711454-001 |
| Copper(II) chloride (CuCl$_2$) | Millipore Sigma | Cat# 451665-5G |
| Chymostatin | Roche | Cat# 11004638001 |
| Dithiothreitol (DTT) | Bio-Rad | Cat# 1610611 |
| Ethylenediaminetetraacetic acid (EDTA) | Millipore Sigma | Cat# E4884-500 |
| Ethylene glycol-bis(β-aminoethyl ether)-N,N,N',N'-tetraacetic 2acid (EGTA) | Millipore Sigma | Cat# E8145 |
| FastDigest NcoI | Thermo Fisher | Cat# FD0574 |
| FastDigest XhoI | Thermo Fisher | Cat# FD0695 |
| Formamide | Millipore Sigma | Cat# F9037 |
| Guanidine-HCl | Thermo Fisher | Cat# BP178-1 |
| Glycerol | Thermo Fisher | Cat# 15514-029 |
| HEPES | Millipore Sigma | Cat# H3375-1KG |
| Hydrochloric acid (HCl) | Thermo Fisher | Cat# A144-500 |
| Hydrogen peroxide (H$_2$O$_2$) | Millipore Sigma | Cat# 16911-250ML-F |
| Lambda Phage DNA | NEB | Cat# N3011L |
| Leupeptin | Millipore Sigma | Cat# 62070-10MG-F |

| REAGENT or RESOURCE | SOURCE | IDENTIFIER |
| --- | --- | --- |
| D-(+)-Maltose Monohydrate | Thermo Fisher | Cat# BP684500 |
| N-(1,10-phenanthroline-5-yl)iodoacetamide (OP) | Biotium | Cat# 92015 |
| NP-40 | Thermo Fisher | Cat# 50152368 |
| Pepstatin A | Millipore Sigma | Cat# 77170-10MG |
| Phenol:chloroform:isoamyl alcohol (25:24:1) | Thermo Fisher | Cat# AC327115000 |
| Phenylmethylsulfonyl fluoride (PMSF) | Millipore Sigma | Cat# 1359061001 |
| QuikChange site-directed mutagenesis kit | Agilent | Cat# 200519 |
| *S.c.* Hta1 | This Paper | N/A |
| *S.c.* Htb1 | This Paper | N/A |
| *S.c.* Hht2 | This Paper | N/A |
| *S.c.* Hhf2 | This Paper | N/A |
| *S.c.* Htz1 | This Paper | N/A |
| *S.c.* htz1 (V83C) | This Paper | N/A |
| *S.c.* htz1(L19C) | This Paper | N/A |
| *S.c.* Htb1-3xFLAG | This Paper | N/A |
| *S.c.* Nap1 | Carl Wu | N/A |
| Sodium acetate | Millipore Sigma | Cat# S2889 |
| Sodium chloride | Millipore Sigma | Cat# BP358-10 |
| Sodium dodecyl sulfate | Millipore Sigma | Cat# L3771-1 |
| SYBR Gold nucleic acid gel stain | Thermo Fisher | Cat# S11494 |
| SYPRO Ruby protein gel stain | Thermo Fisher | Cat# S12000 |
| Taq polymerase | This Paper | N/A |
| Tris-(2-Carboxyethyl)phosphine, Hydrochloride (TCEP) | Thermo Fisher | Cat# T2556-1G |
| Trizma Base | Millipore Sigma | Cat# T1503-1KG |
| Uracil-specific excision reagent (USER Enzyme) | NEB | Cat# M5505L |
| **Experimental Models: Organisms/Strains** | | |
| W1588-4C *SWR1-3xFLAG-loxP* | This Paper | yEL168 |
| W1588-4C *SWR1-3xFLAG-loxP-kanMX-loxP htz1 ::natMX* | Sun and Luk, 2017 | yEL190 |
| W1588-4C *SWR1-3xFLAG-loxP RVB1-MBP-loxP* | This Paper | yEL410 |
| W1588-4C *SWR1-3xFLAG-loxP RVB1-MBP-loxP htz1 ::kanMX* | This Paper | yEL427 |

| REAGENT or RESOURCE | SOURCE | IDENTIFIER |
|---|---|---|
| Oligonucleotides | | |
| Information given in Table S1 | N/A | N/A |
| Recombinant DNA | | |
| pET28a | Novagen | Cat# 69864-3 |
| pET28a-*HTB1-3xFLAG* | Sun and Luk, 2017 | pEL033 |
| pET28a-*HTZ1* | Sun and Luk, 2017 | pEL350 |
| pET28a-*htz1(L19C)* | This Paper | pEL542 |
| pET28a-*htz1(V83C)* | This Paper | pEL543 |
| pUC57-Widom-601-(c1) | Segal et al., 2006; GenScript | pEL550 |
| Widom [Flipped] | Segal et al., 2006 | gEL028 |
| Widom [SHL3-swap] | Winger and Bowman, 2017 | gEL038 |
| Widom [TA+2] | Winger and Bowman, 2017 | gEL040 |
| Software and algorithms | | |
| ImageJ v1.51 | NIH | https://imagej.nih.gov/ij/ |
| ImageQuant TL 7.0 | GE Healthcare | N/A |
| ChimeraX | Goddard et al., 2018 | https://www.cgl.ucsf.edu/chimerax/ |
| Bedtools | V2.28.0 | https://bedtools.readthedocs.io/en/latest |
| Nucleotide_pattern_tri_CG_v3.py | This Paper | N/A |
| Other | | |
| 0.22 mM PVDF membrane | Millipore Sigma | Cat# UFC40GV0S |
| 10 kD MWCO Amicon Ultra-0.5 column | Millipore Sigma | Cat# UFC501024 |
| 10 kD MWCO Amicon Ultra-4 column | Millipore Sigma | Cat# UFC801024 |
| PD SpinTrap G-25 column | Thermo Fisher | Cat# 28-9180-04 |
| Freezer Mill | SPEX SamplePrep | Cat# 6870 |
| Superdex-200 Increase 10/300 GL | GE Healthcare | Cat# GE28-9909-44 |
| Superdex-200 prep grade (XK16/70) | GE Healthcare | Cat# GE17-1043-01 |
| SW-28 Ti rotor | Beckman Coulter | Cat# 342207 |
| SW-55 Ti rotor | Beckman Coulter | Cat# 342194 |
| Typhoon FLA 9500 scanner | GE Healthcare | Cat# 28-9558-08 |